

## The Effect of a Non-universal Extinction Curve on the Wesenheit Function and Cepheid Distances

DOROTA M. SKOWRON ,<sup>1</sup> M. FOUESNEAU ,<sup>2</sup> R. DRIMMEL ,<sup>3</sup> AND S. KHANNA <sup>3</sup>

<sup>1</sup> *Astronomical Observatory, University of Warsaw, Aleje Ujazdowskie 4, 00-478 Warsaw, Poland*

<sup>2</sup> *Max Planck Institute for Astronomy, Königstuhl 17, 69117 Heidelberg, Germany*

<sup>3</sup> *INAF - Osservatorio Astrofisico di Torino, via Osservatorio 20, 10025 Pino Torinese (TO), Italy*

### ABSTRACT

The Wesenheit function is widely used to reduce the effects of interstellar reddening in distance measurements. Its construction, however, relies on the assumption of a universal extinction curve and on fixed values of the total-to-selective extinction ratio,  $R_V$ . Recent studies have shown that  $R_V$  varies significantly across the Milky Way and between different galaxies, raising concerns about systematic biases in Wesenheit magnitudes and period–Wesenheit relations. In this work, we discuss the impact of non-universal extinction on Wesenheit indices by combining the  $R_V$ -dependent extinction curve with a grid of stellar atmosphere models. We compute the integrated extinction in optical and near-infrared passbands, derive  $R_V$ -dependent  $R$  coefficients for multiple Wesenheit indices, and examine how changes in  $R_V$  propagate into Wesenheit magnitudes and Cepheid distances in our Galaxy. We find that the  $R$  coefficients in the Wesenheit functions vary strongly with  $R_V$ . For classical Cepheids in the Milky Way disk, variations of  $R_V$  within the typical observed range (2.6 – 3.6) can lead to substantial differences in the Wesenheit function, reaching  $\pm 0.7$  mag from the mean for the Gaia-based Wesenheit index  $W_G$  and resulting in distance errors of almost 40%. Near-infrared Wesenheit indices are much less sensitive to  $R_V$  changes. Our results clearly show that accounting for variable  $R_V$  is essential when applying period–Wesenheit relations, particularly in the optical regime, or that near or mid infrared based distances should be used. While we present this effect for classical Cepheids, it applies to all pulsating stars for which period–Wesenheit relations are used to infer distances.

**Keywords:** Interstellar extinction (841) – Interstellar reddening (853) – Reddening law (1377) – Magnitude (999) – Pulsating variable stars (1307) – Cepheid distance (1595)

### 1. INTRODUCTION

The Wesenheit<sup>4</sup> function,  $W$ , is an expression for the magnitude of a star that is free of interstellar extinction and reddening. It was conceptually introduced by S. van den Bergh (1975), although the idea of constructing a reddening-free magnitude traces back to H. L. Johnson & W. W. Morgan (1953). The term “Wesenheit” itself was later introduced by B. F. Madore (1982), who also explored its detailed properties and applications, using it to calibrate the period–luminosity relation for classical Cepheids. A comprehensive historical overview of the development and evolution of the Wesenheit function, as well as its underlying physical basis can be found in B. F. Madore & W. L. Freedman (2024).

Email: dszczyg@astrouw.edu.pl

<sup>4</sup> Wesenheit is a German word for “intrinsic essence”

While the Wesenheit function can be applied to any type of star, it has been used primarily as a luminosity indicator in the period–luminosity (PL) relation for pulsating stars, such as Cepheids, RR Lyrae, or long-period variables. This relation, expressed as  $W = a \log P + b$ , is commonly referred to as the period–Wesenheit (PW) relation. Its use significantly reduces the scatter relative to the standard PL relation by effectively accounting for interstellar extinction (see Fig. 6 in I. Soszyński et al. 2008). This is particularly important in the case of classical Cepheids, which serve as standard candles for measuring precise distances within the Milky Way and in galaxies well beyond the Local Group, making them excellent tracers of young stellar populations and key contributors to the calibration of the cosmic distance scale and the determination of the Hubble constant (H0DN Collaboration et al. 2025). Therefore, the subsequent analysis will be focused on classical Cepheid variable stars.

The main assumption in constructing the Wesenheit function is that the ratio of total-to-selective extinction,  $R$ , is *universal within a galaxy and known a priori* (i.e., a universal extinction curve). Otherwise, if  $R$  is not correct or not universal, the Wesenheit magnitude will not be reddening-free. In the optical, the most commonly used total-to-selective extinction ratio is

$$R_V = \frac{A_V}{E(B-V)} = \frac{A_V}{A_B - A_V}, \quad (1)$$

which is assumed to have a constant mean value of around 3.1 in the Milky Way (e.g., [G. V. Schultz & W. Wiemer 1975](#); [E. L. Fitzpatrick 1999](#)). However, growing evidence indicates that  $R_V$  is not constant within the Galaxy, but it varies significantly, particularly in regions of high extinction ([E. L. Fitzpatrick & D. Massa 2007](#); [E. F. Schlafly et al. 2016](#); [D. M. Nataf et al. 2016](#); [J. Maíz Apellániz & R. H. Barbá 2018](#); [M. Fouesneau et al. 2022](#); [R. Zhang et al. 2023](#); [X. Zhang & G. M. Green 2025](#)). This is especially important for classical Cepheids, which belong to the young population and are therefore confined to the Galactic disk, where the extinction is highest. The adverse consequences of a variable  $R_V$  on Cepheid distance estimates for Galactic structure studies have already been reported by [D. M. Skowron et al. \(2025\)](#), and this letter aims to explore this effect in greater detail.

In the following section, we describe the Wesenheit function and how it is defined for a given set of passbands, including the  $R$  coefficient. Section 3 details how we apply the extinction curve to derive extinctions for a variety of passbands for different values of  $R_V$ . Section 4 investigates the effect of a variable  $R_V$  on the Wesenheit magnitudes and distances, and we summarize our conclusions in Section 5.

## 2. THE WESENHEIT FUNCTION DEFINITIONS

The Wesenheit function (also called the Wesenheit index or the Wesenheit magnitude) is traditionally calculated from apparent magnitudes at two different passbands characterised by wavelengths  $\lambda_1$  and  $\lambda_2$ , as:

$$W_{\lambda_1, \lambda_2} = m_{\lambda_2} - R_{\lambda_1, \lambda_2} \times (m_{\lambda_1} - m_{\lambda_2}) \quad (2)$$

where  $R_{\lambda_1, \lambda_2}$  is the ratio of total-to-selective extinction:

$$R_{\lambda_1, \lambda_2} = \frac{A_{\lambda_2}}{E(m_{\lambda_1} - m_{\lambda_2})} = \frac{A_{\lambda_2}}{A_{\lambda_1} - A_{\lambda_2}} \quad (3)$$

with  $A_{\lambda}$  denoting the extinction and  $E(m_{\lambda_1} - m_{\lambda_2})$  representing the color excess. Another representation of the Wesenheit magnitude is composed of three passbands:

$$W_{\lambda_1, \lambda_2, \lambda_3} = m_{\lambda_3} - R_{\lambda_1, \lambda_2, \lambda_3} \times (m_{\lambda_2} - m_{\lambda_3}) \quad (4)$$

where:

$$R_{\lambda_1, \lambda_2, \lambda_3} = \frac{A_{\lambda_1}}{E(m_{\lambda_2} - m_{\lambda_3})} = \frac{A_{\lambda_1}}{A_{\lambda_2} - A_{\lambda_3}} \quad (5)$$

In practice, the choice of which Wesenheit index to use is dictated by the passbands for which observational data are available. Traditionally,  $B$  and  $V$  bands have been employed; however, following the publication of catalogs containing over 9,500 Cepheids in the Magellanic Clouds by the Optical Gravitational Lensing Experiment (OGLE), the  $V$  and  $I$  bands have become widely adopted ([I. Soszyński et al. 2008, 2015](#)), while additional observations from near-IR surveys have led to the use of a variety of Wesenheit indices that combine the  $V$ ,  $J$ ,  $H$ , and  $K_S$  magnitudes. The use of classical Cepheids as standard candles, where distance measurements are based on Hubble Space Telescope (HST) observations in the optical ( $V = F555W$ ,  $I = F814W$ ) and near-infrared ( $H = F160W$ ) bands, relies on the near-IR Wesenheit index,  $W_H$ , constructed from these three HST passbands ([A. G. Riess et al. 2009](#)). With the availability of all-sky data for classical Cepheids from the Gaia mission, the Wesenheit magnitude  $W_G$  was introduced, with the three-band variant exhibiting the lowest scatter ([V. Ripepi et al. 2019](#)).

In the following analysis, we focus on the most often used Wesenheit functions, listed in Table 1, although numerous other combinations have also been studied (e.g. [L. Inno et al. 2016](#); [L. Breuval et al. 2022](#); [A. Bhardwaj et al. 2024](#)).

## 3. EXTINCTION CURVE

To calculate the  $R$  coefficient in different bands, we need to assume a relation between interstellar dust extinction and wavelength. Commonly used  $R_V$  dependent extinction curves in the Milky Way include those of [J. A. Cardelli et al. \(1989\)](#) and [E. L. Fitzpatrick \(1999\)](#), and more recently [K. D. Gordon et al. \(2009\)](#); [E. L. Fitzpatrick et al. \(2019\)](#); [K. D. Gordon et al. \(2021\)](#); [M. Decleir et al. \(2022\)](#); [X. Zhang & G. M. Green \(2025\)](#), which cover various wavelength ranges. However, because these studies used different samples, methods, and wavelength ranges, combining the resulting extinction curves to cover the full ultraviolet-mid-infrared range could introduce artificial discontinuities between wavelength regions. Therefore, for the following analysis, we adopt the extinction curve of [K. D. Gordon et al. \(2023](#), hereafter G23), which is the first  $R_V$  dependent extinction relation valid over the full wavelength range.

G23 define an extinction curve normalized to the monochromatic extinction at 550 nm. However, we stress that the wavelength dependence of their extinc-

**Table 1.** Wesenheit index definitions used in various studies and calculated in this study using the extinction curve of K. D. Gordon et al. (2023).

Wesenheit index	$R$ definition	$R$ value	$R$ origin
$W_{VI} = I - R_{VI}(V - I)$	$R_{VI} = A_I/E(V - I)$	1.55	$R_V = 3.23$ , J. A. Cardelli et al. (1989)
		1.387	$R_V = 3.1$ , E. L. Fitzpatrick (1999)
		1.335	$R_V = 3.1$ , K. D. Gordon et al. (2023)
$W_{JK} = K - R_{JK}(J - K)$	$R_{JK} = A_K/E(J - K)$	0.679	$R_V = 3.1$ , J. A. Cardelli et al. (1989)
		0.688	$R_V = 3.23$ , J. A. Cardelli et al. (1989)
		0.553	$R_V = 3.1$ , K. D. Gordon et al. (2023)
$W_{VK} = K - R_{VK}(V - K)$	$R_{VK} = A_K/E(V - K)$	0.129	$R_V = 3.23$ , J. A. Cardelli et al. (1989)
		0.090	$R_V = 3.1$ , K. D. Gordon et al. (2023)
$W_H = H - R_H(V - I)$	$R_H = A_H/E(V - I)$	0.365	$R_V = 3.1$ , J. A. Cardelli et al. (1989)
		0.35	$R_V = 3.1$ , E. L. Fitzpatrick (1999)
		0.321	$R_V = 3.1$ , K. D. Gordon et al. (2023)
$W_G = G - R_G(G_{BP} - G_{RP})$	$R_G = A_G/E(G_{BP} - G_{RP})$	1.9	empirical, V. Ripepi et al. (2019)
		1.67	$R_V = 3.1$ , K. D. Gordon et al. (2023)

tion curve in the optical range does not differ significantly from past formulations (e.g., E. L. Fitzpatrick 1999; E. L. Fitzpatrick et al. 2019). Nevertheless, their normalization to a monochromatic extinction leads to differences that we highlight below.

To avoid confusing notations and to make a clear distinction between measured quantities and model parameters, we will henceforth denote  $A_0$  and  $R_0$  for the extinction and total-to-selective extinction ratio parameters of the G23 extinction curve, respectively, and reserve the notation  $A_X$ ,  $R_X$  for integrated effects within a given passband  $X$  (or monochromatic measurements).

For a star of spectral energy distribution  $f_\lambda$  and the G23 extinction curve  $A_\lambda(A_0, R_0)$ , we define the attenuation in the passband  $X$  of throughput  $T_X$  as

$$A_X = -2.5 \log_{10} \frac{\int \gamma_X(\lambda) T_X(\lambda) f_\lambda e^{-A_\lambda} d\lambda}{\int \gamma_X(\lambda) T_X(\lambda) f_\lambda d\lambda}, \quad (6)$$

with  $\gamma_X(\lambda) = 1$  for energy-counting (e.g., Johnson  $B$ ,  $V$ ,  $I$  bands), or  $\gamma_X(\lambda) = \lambda/(hc)$  for photon-counting (e.g., Gaia  $G$ ,  $G_{BP}$ ,  $G_{RP}$ ; 2MASS  $J$ ,  $H$ ,  $K_s$ ) photometric system. As  $A_X$  is not the weighted average monochromatic extinction through  $T_X$ , we must calculate the integrated effect for any spectrum of interest.

We used the Atlas-9 (2004; F. Castelli & R. L. Kurucz 2003) atmosphere library to compute a grid of 17,603 stellar spectra references spanning effective temperatures  $T_{\text{eff}} \in [2,500; 8,000]$  K, surface gravities  $\log g \in [-0.5; 5.5]$  dex, and metallicities  $[M/H] \in [-5; +1]$  dex. We expand this collection by applying the G23 extinction curve on a grid of  $A_0 \in [0, 10.0]$  by step of 0.5 mag and  $R_0 \in [2.3, 2.6, 3.1, 3.6, 4.1, 4.6, 5.1, 5.6]$ . Finally, we

use Pyphot (M. Fouesneau 2025) to compute the photometric calculations in the relevant passbands for the present work, namely: Johnson  $B$  &  $V$ ; Cousins  $I$ ; Gaia DR3  $G$ ,  $G_{BP}$ ,  $G_{RP}$  and 2MASS  $J$ ,  $H$ ,  $K_s$ .<sup>5</sup>

It is important to note that the  $R_0$  parameter that controls the slope of the extinction curve in G23<sup>6</sup> is not equivalent to  $R_V$ . In the past, this extinction parameter was often “calibrated” using actual photometric  $R_V$  measurements, so that  $R_0$  was approximately equal to  $R_V$ . However, in the case of G23, the parameter  $R_0$  is calibrated on spectroscopic measurements of  $R_{55} = A(550)/(A(440) - A(550))$ , where  $A(550)$  and  $A(440)$  are the monochromatic extinctions at 440 and 550 nm, leading to a substantial offset with respect to  $R_V$ . To illustrate this offset and the dependence of  $R_V$  on the source spectra, Figure 1 shows how  $R_V$  varies with respect to the effective temperature for stars and different  $\log g$ , for a fixed extinction curve with  $R_0 = 3.1$ . We note that at the typical temperature of Cepheids ( $T_{\text{eff}} = 5500$  K), and for hotter stars, the variation in  $R_V$  is minor, while the variation in  $R_V$  for stars cooler than about 5000 K, which includes giants and lower main sequence stars, can be quite large.

In Figure 2 (upper panel), we show the relation between  $R_V$  and  $R_0$  for three different stellar types, including a typical Cepheid ( $T_{\text{eff}} = 5500$  K,  $\log g = 1.5$ ). In

<sup>5</sup> We took the transmission curves from the SVO-profile service: <http://svo2.cab.inta-csic.es/theory/fps/>; C. Rodrigo & E. Solano (2020)

<sup>6</sup> Referred to as “ $R(V)$ ” in their paper, and as “ $R_V$ ” in their python package.

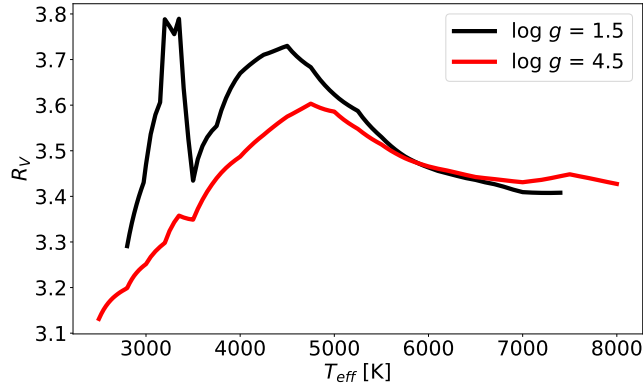


**Figure 1.**  $R_V$  as a function of effective temperature  $T_{\text{eff}}$  for giants ( $\log g = 1.5$ ) and main sequence stars ( $\log g = 4.5$ ), assuming a G23 extinction curve with  $R_0 = 3.1$ .

each case, we show the relation for  $0.5 < A_0 < 9.5$  mag with the spread indicated by the shaded regions, and the median indicated by points. There is an apparent offset between  $R_V$  and  $R_0$  which we characterize by fitting a second-order polynomial to the median points, finding:

$$R_V = 0.2267 + 1.145 R_0 - 0.021 R_0^2 \quad (7)$$

where the coefficients have uncertainties of no more than 2%, and they remain unchanged within  $T_{\text{eff}}$  and  $\log g$  range typical for Cepheids. While this offset remains nearly constant as  $R_0$  is varied, the lower panel of Figure 2 shows the ratio  $R_V/R_0$  to highlight the subtle variation with respect to  $R_0$ , where the shaded region illustrates the uncertainty in the ratio from our polynomial fit. Because the parameter  $R_0$  is calibrated on measurements of  $R_{55}$ , we found that the offset of  $R_0$  with respect to  $R_V$  (Eq. 7) is quite similar to the offset of  $R_{55}$  with respect to  $R_V$ , as specified by [X. Zhang & G. M. Green \(2025\)](#), i.e.  $R_V = 1.1 R_{55} + 0.07$ .

#### 4. DISCUSSION

Recently [X. Zhang & G. M. Green \(2025\)](#) measured the  $R_V$  parameter within the Milky Way and the Magellanic Clouds using low-resolution optical spectra from *Gaia* for  $\sim 130$  million stars. The resulting three-dimensional maps provide  $R_V$  values as a function of distance, enabling more accurate extinction corrections than those obtained by assuming a constant  $R_V$  value. The mean differential  $R_V$  value in the Galaxy is 3.11 with a  $1\sigma$  range from 2.60 to 3.88, and the average integrated  $R_V$  is 3.08 with a  $1\sigma$  range from 2.86 to 3.28, although values as low as 2.00 and as high as 8.00 are observed. Both average estimates are consistent with  $R_V = 3.1$ , as found in many previous studies of the Milky Way. This section shows how varying extinction curve, as parameterized by  $R_V$ , affects the Wesenheit

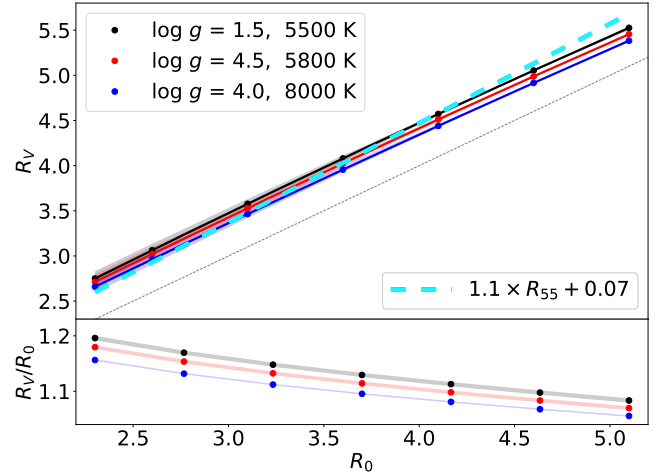


**Figure 2.**  $R_V$  as a function of  $R_0$ , shown for three different types of stars. In the upper panel, the shaded region captures the spread over  $0.5 < A_0 < 9.5$ , while the points are the median values. The black solid curve is the best-fit polynomial for Cepheids (Eq. 7), while the cyan line is the proposed relation between  $R_V$  and  $R_{55}$  of [X. Zhang & G. M. Green \(2025\)](#). The grey dotted line indicates the identity relation. The lower panel shows the ratio  $R_V/R_0$  with the spread capturing the uncertainty in the polynomial fit.

magnitudes and distances based on PW relations. That is, we fix the extinction curve using a specific value of the parameter  $R_0$ , but in this section translate these  $R_0$  values to the more commonly used  $R_V$  parameter used in the past to parameterize extinction curves, using Eq. 7 specific to Cepheids.

#### 4.1. The impact of $R_V$ on the $R$ coefficient

The Wesenheit index parameter  $R$  quantifies the ratio of total to selective extinction for a given combination of passbands (Eqns. 3,5) and therefore varies across specific definitions of the Wesenheit index. Figure 3 shows the  $R$  coefficient as a function of the color excess  $E$ , where each panel corresponds to a different definition of  $W$  and  $R$ , listed in Table 1. The color coding in each panel represents distinct  $R_V$  values, and the grey dotted line marks the reddening values typical for Milky Way Cepheids. Light-green dashed lines represent  $R$ , when instead of G23, the [E. L. Fitzpatrick \(1999\)](#) extinction curve for  $R_V = 3.1$  is used, and black dashed lines show constant values used in the literature.

First, it is worth noting that for most definitions of  $R$ , the lines corresponding to different  $R_V$  values are not horizontal, i.e., they depend on the reddening. This indicates that, despite common understanding,  $R$  is not constant over reddening for a fixed extinction curve, as reddening is not perfectly proportional to extinction. This effect is most pronounced for the Gaia coefficient

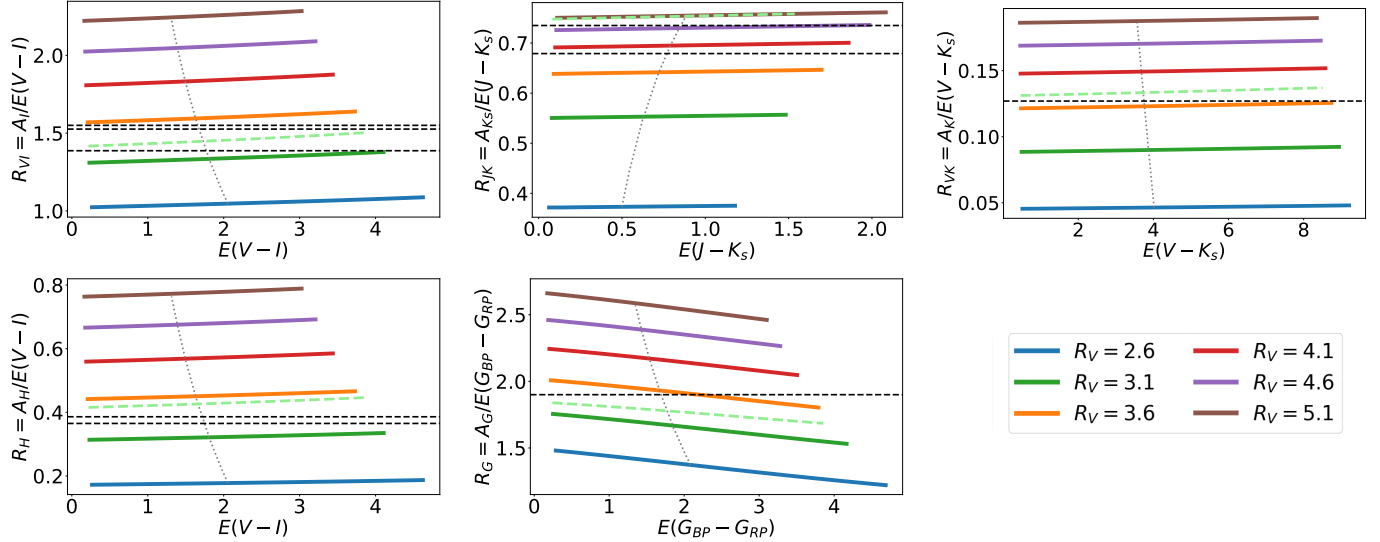


**Figure 3.** The dependence of the  $R$  coefficient, used in the definition of a given Wesenheit index, on  $R_V$ , as a function of the color excess  $E$  for various passbands, calculated using a typical Cepheid source spectra. Colors mark different  $R_V$  values, according to the legend. Solid lines assume the G23 extinction curve, while the light-green dashed line is the E. L. Fitzpatrick (1999) extinction curve, but only for  $R_V = 3.1$ . Black dashed lines show constant  $R$  coefficients adopted in various studies, and the grey dotted line represents reddening values typical for Milky Way Cepheids.

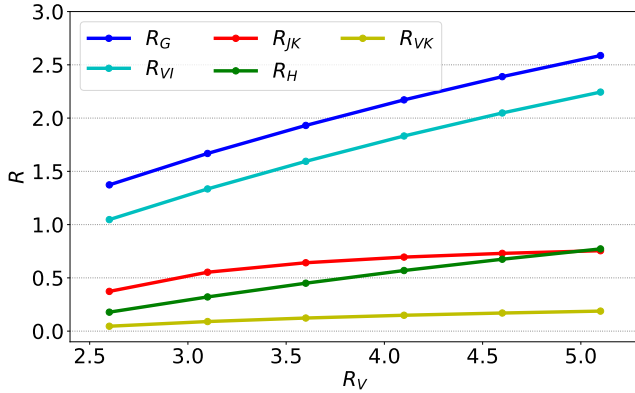


**Figure 4.** The  $R$  parameter used in the definition of various Wesenheit indices as a function of  $R_V$ . Each color represents a different Wesenheit index parameter  $R$ , defined in Table 1, and plotted in Figure 3.

$R_G$  where the colored lines exhibit the highest slope, due to the large width of the Gaia passbands.

However, a more important conclusion from Figure 3 is that the value of  $R$  varies significantly with  $R_V$ . For example, in the first panel of this figure, we see that for a typical Cepheid reddening (indicated by the gray dotted line), the value of  $R_{VI}$  changes from 1.05 to 1.6 for  $R_V$  varying from 2.6 to 3.6, which is a typical  $R_V$  range in the Milky Way. In Section 4.2 we will show how this impacts the Wesenheit magnitude and the resulting distance determinations.

In Figure 4, we summarize plots from Figure 3, by showing how the  $R$  coefficient changes with  $R_V$  for different Wesenheit functions. Each line corresponds to one panel from Figure 3, assuming a mean Cepheid reddening as indicated by the grey dotted lines.

#### 4.2. The impact of $R_V$ on the Wesenheit magnitude and distance

Following the results of X. Zhang & G. M. Green (2025), we adopt the mean value of  $R_V = 3.1 \pm 0.22$ . Then  $R_V = 2.6$  and  $R_V = 3.6$ , which represent a typical  $R_V$  range in the Milky Way, are a good approximation of the  $\pm 2\sigma$  range around the mean of the integrated  $R_V$ <sup>7</sup> (see their Figure S8). In that case, the relative difference in the  $R$  parameter within  $R_V = 3.1 \pm 0.22$ , estimated from Figure 4, is roughly 8.5%, 10%, 12%, 21%, and 21.5% for  $R_G$ ,  $R_{VI}$ ,  $R_{JK}$ ,  $R_H$ , and  $R_{VK}$ , respectively.

However, the final value of the Wesenheit magnitude depends not only on its  $R$  coefficient, but also on the color of the star (Eqn. 2). Therefore, to estimate how the Wesenheit magnitude of a given star would change with the change of  $R_V$ , we have to account for both factors. To do so, we calculate Wesenheit magnitudes at different values of  $R_V$  (estimating the adequate  $R_{\lambda_1, \lambda_2}^{R_V}$  coefficients based on relations plotted in Figure 4), and

<sup>7</sup> X. Zhang & G. M. Green (2025) provide maps for both differential, and integrated along a line-of-sight to a specific distance,  $R_{55}$ , from which the integrated  $R_V$  (Eq. 1) can be derived.

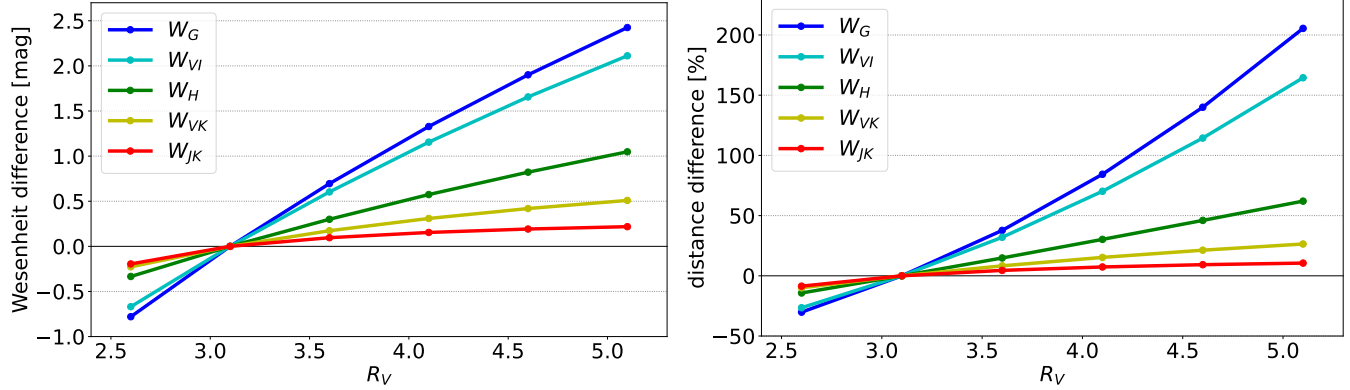


**Figure 5.** The effect of  $R_V$  on the Wesenheit index (left, Eqn. 8) and distance (right, Eqn. 9), relative to values at  $R_V = 3.1$ . Each color represents a different Wesenheit function  $W$ , defined in Table 1, according to the legend. Points are at  $R_V$  values of 2.6, 3.1, 3.6, 4.1, 4.6, 5.1.

at  $R_V = 3.1$ :

$$W_{\lambda_1, \lambda_2} = m_{\lambda_2} - R_{\lambda_1, \lambda_2}^{R_V} \times (m_{\lambda_1} - m_{\lambda_2})$$

$$W_{\lambda_1, \lambda_2}^{3.1} = m_{\lambda_2} - R_{\lambda_1, \lambda_2}^{3.1} \times (m_{\lambda_1} - m_{\lambda_2})$$

and then their difference:

$$W_{\lambda_1, \lambda_2} - W_{\lambda_1, \lambda_2}^{3.1} = (R_{\lambda_1, \lambda_2}^{3.1} - R_{\lambda_1, \lambda_2}^{R_V}) \times (m_{\lambda_1} - m_{\lambda_2}) \quad (8)$$

For the color term, we use mean colors and standard deviations of Milky Way Cepheids, which in the considered passband combinations are:  $(V - I) = 2.32 \pm 0.95$  mag,  $(G_{BP} - G_{RP}) = 2.64 \pm 1.12$  mag,  $(V - K) = 5.22 \pm 2.14$  mag, and  $(J - K) = 1.08 \pm 0.47$  mag. We use these numbers together with  $R_{\lambda_1, \lambda_2}$  coefficients for a given  $R_V$  value to plot the change in the Wesenheit index as a function of  $R_V$  (Eqn. 8), in the left panel of Figure 5, where colors represent different Wesenheit functions. The right panel shows the resulting change in distance, relative to the distance calculated assuming  $R_V = 3.1$ , as:

$$\Delta d/d = 10^{0.2(W_{\lambda_1, \lambda_2} - W_{\lambda_1, \lambda_2}^{3.1})} - 1 \quad (9)$$

Since we calculate the change in  $W$  and distance with respect to  $R_V = 3.1$ , all lines cross at zero for  $R_V = 3.1$ .

The largest differences are observed for the Gaia-based Wesenheit index,  $W_G$ , where a change within  $R_V = 3.1 \pm 0.22$  results in  $\pm 0.37$  mag difference in  $W_G$ , which translates to  $\pm 17\%$  change in distance. When considering the typically observed range of  $(2.6 - 3.6)$ , the discrepancies are more pronounced, e.g., for the  $R_V$  change between 3.1 and 3.6, the difference is 0.7 mag in  $W_G$ , which translates to 38% distance change. In the case of the  $W_H$  index, the change within  $R_V = 3.1 \pm 0.22$  is  $\pm 0.16$  mag in  $W$  and  $\pm 7.5\%$  in distance, while the change between 3.1 and 3.6 is 0.30 mag in  $W$  and 15% in distance. The smallest effect of variable  $R_V$  is observed for the near-infrared  $W_{JK}$  index (0.1 mag and

4.5% in distance between  $R_V = 3.1$  and 3.6), which is not surprising, as the extinction is much smaller at infrared wavelengths than in the optical.

## 5. CONCLUSIONS

The analysis presented in this work demonstrates that the long-standing assumption of a universal extinction curve, expressed as a fixed value of  $R_V$ , has an underestimated negative impact on the Wesenheit magnitudes and PW-based distance estimates. Using recent measurements of spatially varying  $R_V$ , we show that these variations introduce significant systematics in Cepheid Wesenheit magnitudes and distances.

Milky Way classical Cepheids are especially affected because they lie in the Galactic disk, where extinction is both high and highly variable. As a result, even moderate changes in  $R_V$  produce noticeable shifts in the  $R$  coefficients used in optical Wesenheit relations. For Gaia-based Wesenheit magnitudes,  $W_G$ , a shift from  $R_V = 3.1$  to  $R_V = 3.6$  leads to changes of  $\approx 0.7$  mag in  $W_G$ , corresponding to distance differences of almost 40%. These shifts are large enough to explain the strong discrepancies found by D. M. Skowron et al. (2025) between Milky Way Cepheid distances derived from Gaia photometry and those obtained from mid-infrared PL relations combined with extinction maps. Near-infrared Wesenheit indices remain the least affected and therefore offer the most reliable distances.

PW relations constructed with different Wesenheit indices are also widely used for distance measurements in other galaxies, most notably in the Magellanic Clouds. As shown by X. Zhang & G. M. Green (2025), the mean  $R_V$  in the SMC is lower than in the Milky Way, while in the LMC, the range of  $R_V$  is much wider. Because the choice of  $R$  directly affects the definition of the Wesenheit function, adopting an  $R_V$  appropriate for one galaxy but applying it to another will change the slope

and zero point of the PW relation, and therefore alter the inferred distances. This would also affect the calibration of the extragalactic distance scale and, in consequence, influence measurements of the Hubble constant. For example, A. G. Riess et al. (2016) showed that  $R$  variations arising from changing between the reddening laws of E. L. Fitzpatrick (1999) and J. A. Cardelli et al. (1989) result in  $H_0$  changing by  $0.1 - 0.15 \text{ km s}^{-1} \text{ Mpc}^{-1}$  when  $W_H$  is used, and by  $-2.15 - 3.8 \text{ km s}^{-1} \text{ Mpc}^{-1}$  when  $W_{VI}$  is used, demonstrating that near-infrared data remains the preferred choice for  $H_0$  studies, in the absence of individual  $R$  values.

The main conclusion of this work is that optical Wesenheit indices of Milky Way Cepheids are not “reddening-free”, as the assumption of a universal extinction curve is not satisfied. However, a positive consequence is that the colors of highly reddened Cepheids contain information of  $R_V$  on large scales, as will be demonstrated in R. Drimmel et al. (2025, in prep.). It is also important to note, that although our discussion focuses on classical Cepheids, the same considerations are valid for all classes of pulsating stars, such as RR Lyrae or long-period variables, for which PW relations are employed to derive distances.

## 6. SOFTWARE AND THIRD PARTY DATA REPOSITORY CITATIONS

*Software:* `scipy` (P. Virtanen et al. 2020), `numpy` (C. R. Harris et al. 2020), `matplotlib` (J. D. Hunter 2007), Jupyter notebooks (T. Kluyver et al. 2016), `Pyphot` (M. Fouesneau 2025),

## ACKNOWLEDGMENTS

DMS acknowledges support from the European Union (ERC, LSP-MIST, 101040160). SK acknowledges support from the European Union’s Horizon 2020 research and innovation program under the GaiaUnlimited project (grant agreement No 101004110). Views and opinions expressed are, however, those of the authors only and do not necessarily reflect those of the European Union or the European Research Council. Neither the European Union nor the granting authority can be held responsible for them. RD & EP are supported in part by the Italian Space Agency (ASI) through contract 2025-10-HH.0 to the National Institute for Astrophysics (INAF). This work made use of the Overleaf platform and the NASA Astrophysics Data System.

## REFERENCES

Bhardwaj, A., Ripepi, V., Testa, V., et al. 2024, A&A, 683, A234, doi: [10.1051/0004-6361/202348140](https://doi.org/10.1051/0004-6361/202348140)

Breuval, L., Riess, A. G., Kervella, P., Anderson, R. I., & Romaniello, M. 2022, ApJ, 939, 89, doi: [10.3847/1538-4357/ac97e2](https://doi.org/10.3847/1538-4357/ac97e2)

Cardelli, J. A., Clayton, G. C., & Mathis, J. S. 1989, ApJ, 345, 245, doi: [10.1086/167900](https://doi.org/10.1086/167900)

Castelli, F., & Kurucz, R. L. 2003, in IAU Symposium, Vol. 210, Modelling of Stellar Atmospheres, ed. N. Piskunov, W. W. Weiss, & D. F. Gray, A20, doi: [10.48550/arXiv.astro-ph/0405087](https://doi.org/10.48550/arXiv.astro-ph/0405087)

Decleir, M., Gordon, K. D., Andrews, J. E., et al. 2022, ApJ, 930, 15, doi: [10.3847/1538-4357/ac5dbe](https://doi.org/10.3847/1538-4357/ac5dbe)

Drimmel, R., Skowron, D. M., Khanna, S., Poggio, E., & Fouesneau, M. 2025, in prep.

Fitzpatrick, E. L. 1999, PASP, 111, 63, doi: [10.1086/316293](https://doi.org/10.1086/316293)

Fitzpatrick, E. L., & Massa, D. 2007, ApJ, 663, 320, doi: [10.1086/518158](https://doi.org/10.1086/518158)

Fitzpatrick, E. L., Massa, D., Gordon, K. D., Bohlin, R., & Clayton, G. C. 2019, ApJ, 886, 108, doi: [10.3847/1538-4357/ab4c3a](https://doi.org/10.3847/1538-4357/ab4c3a)

Fouesneau, M. 2025, `pyphot`, 1.6.0  
<https://github.com/mfouesneau/pyphot>

Fouesneau, M., Andrae, R., Dharmawardena, T., et al. 2022, A&A, 662, A125, doi: [10.1051/0004-6361/202141828](https://doi.org/10.1051/0004-6361/202141828)

Gordon, K. D., Cartledge, S., & Clayton, G. C. 2009, ApJ, 705, 1320, doi: [10.1088/0004-637X/705/2/1320](https://doi.org/10.1088/0004-637X/705/2/1320)

Gordon, K. D., Clayton, G. C., Decleir, M., et al. 2023, ApJ, 950, 86, doi: [10.3847/1538-4357/acccb59](https://doi.org/10.3847/1538-4357/acccb59)

Gordon, K. D., Misselt, K. A., Bouwman, J., et al. 2021, ApJ, 916, 33, doi: [10.3847/1538-4357/ac00b7](https://doi.org/10.3847/1538-4357/ac00b7)

H0DN Collaboration, Casertano, S., Anand, G., et al. 2025, arXiv e-prints, arXiv:2510.23823, doi: [10.48550/arXiv.2510.23823](https://doi.org/10.48550/arXiv.2510.23823)

Harris, C. R., Millman, K. J., van der Walt, S. J., et al. 2020, Nature, 585, 357, doi: [10.1038/s41586-020-2649-2](https://doi.org/10.1038/s41586-020-2649-2)

Hunter, J. D. 2007, Computing in Science & Engineering, 9, 90, doi: [10.1109/MCSE.2007.55](https://doi.org/10.1109/MCSE.2007.55)

Inno, L., Bono, G., Matsunaga, N., et al. 2016, ApJ, 832, 176, doi: [10.3847/0004-637X/832/2/176](https://doi.org/10.3847/0004-637X/832/2/176)

Johnson, H. L., & Morgan, W. W. 1953, ApJ, 117, 313, doi: [10.1086/145697](https://doi.org/10.1086/145697)

Kluyver, T., Ragan-Kelley, B., Pérez, F., et al. 2016, in Positioning and Power in Academic Publishing: Players, Agents and Agendas, ed. F. Loizides & B. Schmidt, IOS Press, 87 – 90

Madore, B. F. 1982, *ApJ*, 253, 575, doi: [10.1086/159659](https://doi.org/10.1086/159659)

Madore, B. F., & Freedman, W. L. 2024, *ApJ*, 961, 166, doi: [10.3847/1538-4357/acfaea](https://doi.org/10.3847/1538-4357/acfaea)

Maíz Apellániz, J., & Barbá, R. H. 2018, *A&A*, 613, A9, doi: [10.1051/0004-6361/201732050](https://doi.org/10.1051/0004-6361/201732050)

Nataf, D. M., Gonzalez, O. A., Casagrande, L., et al. 2016, *MNRAS*, 456, 2692, doi: [10.1093/mnras/stv2843](https://doi.org/10.1093/mnras/stv2843)

Riess, A. G., Macri, L., Casertano, S., et al. 2009, *ApJ*, 699, 539, doi: [10.1088/0004-637X/699/1/539](https://doi.org/10.1088/0004-637X/699/1/539)

Riess, A. G., Macri, L. M., Hoffmann, S. L., et al. 2016, *ApJ*, 826, 56, doi: [10.3847/0004-637X/826/1/56](https://doi.org/10.3847/0004-637X/826/1/56)

Ripepi, V., Molinaro, R., Musella, I., et al. 2019, *A&A*, 625, A14, doi: [10.1051/0004-6361/201834506](https://doi.org/10.1051/0004-6361/201834506)

Rodrigo, C., & Solano, E. 2020, in XIV.0 Scientific Meeting (virtual) of the Spanish Astronomical Society, 182

Schlafly, E. F., Meisner, A. M., Stutz, A. M., et al. 2016, *ApJ*, 821, 78, doi: [10.3847/0004-637X/821/2/78](https://doi.org/10.3847/0004-637X/821/2/78)

Schultz, G. V., & Wiemer, W. 1975, *A&A*, 43, 133

Skowron, D. M., Drimmel, R., Khanna, S., et al. 2025, *ApJS*, 278, 57, doi: [10.3847/1538-4365/adc3f3](https://doi.org/10.3847/1538-4365/adc3f3)

Soszyński, I., Poleski, R., Udalski, A., et al. 2008, *AcA*, 58, 163, doi: [10.48550/arXiv.0808.2210](https://doi.org/10.48550/arXiv.0808.2210)

Soszyński, I., Udalski, A., Szymański, M. K., et al. 2015, *AcA*, 65, 297, doi: [10.48550/arXiv.1601.01318](https://doi.org/10.48550/arXiv.1601.01318)

van den Bergh, S. 1975, in Galaxies and the Universe, ed. A. Sandage, M. Sandage, & J. Kristian, 509

Virtanen, P., Gommers, R., Oliphant, T. E., et al. 2020, *Nature Methods*, 17, 261, doi: [10.1038/s41592-019-0686-2](https://doi.org/10.1038/s41592-019-0686-2)

Zhang, R., Yuan, H., & Chen, B. 2023, *ApJS*, 269, 6, doi: [10.3847/1538-4365/acf764](https://doi.org/10.3847/1538-4365/acf764)

Zhang, X., & Green, G. M. 2025, *Science*, 387, 1209, doi: [10.1126/science.ado9787](https://doi.org/10.1126/science.ado9787)